

Crossed surface flat bands of Weyl semimetal superconductors

Bo Lu, Keiji Yada, Masatoshi Sato, and Yukio Tanaka

Department of Applied Physics, Nagoya University, Nagoya 464-8603, Japan

(Dated: December 6, 2024)

It has been noted that certain surfaces of Weyl semimetals have bound states forming open Fermi arcs, which are never seen in typical metallic states. We show that the Fermi arcs enable them to support an even more exotic surface state with *crossed* flat bands in the superconducting state. We clarify the topological origin of the crossed flat bands and the relevant symmetry that stabilizes the crossing point. We also discuss their possible experimental verification by tunneling spectroscopy.

PACS numbers: 74.50.+r, 73.20.-r, 74.20.Rp, 03.65.Vf

Introduction.— Weyl semimetals (WSMs) are three-dimensional materials that support pairs of bulk gapless points that are effectively described by Weyl fermions [1–9]. The characteristic band-touching points may be viewed as topological magnetic monopoles in momentum space, which predicts many interesting phenomena such as anomalous Hall effects, chiral anomalies [10–14], and magneto-electric effects [15–19]. Candidate materials include pyrochlore iridates [2], HgCr_2Se_4 [3, 20] and magnetically doped Bi_2Se_3 family [7, 21]. A simpler realization in a topological insulator multilayer has also been proposed [4, 22].

The most fundamental and striking prediction for WSMs is the existence of Fermi *arcs* on their boundary [2]. Whereas ordinary electrons in metals form closed Fermi surfaces in momentum space, the surface bound states of WSMs form open arcs at the Fermi energy, not closed circles. The Fermi arcs reported in experimental studies of high- T_c cuprate superconductors were not true arcs but Fermi surfaces with partially enhanced density of states. In contrast, WSMs host true arcs that are terminated by the projection of band-touching Weyl points on the surface Brillouin zone (BZ). Such exotic states may carry topological flows, so they provide the aforementioned variety of nontrivial phenomena in low-energy physics.

In this letter, we show that WSMs may support even more exotic surface bound states when they become superconductors. The novel surface states form *crossed* flat bands, not simple arcs. On the basis of topology, we argue that the existence of crossed flat bands is rather general. Such crossed band structures strongly enhance the surface density of states, which might induce nontrivial low-energy phenomena. Our findings also extend the possibility of designing surface states.

Our work is motivated by recent results on superconductivity in WSMs [23–26]. Upon slight doping, disconnected Fermi surfaces appear, each of which surrounds one of the band-touching Weyl points. Either uniform or nonuniform Cooper pairing can be formed on the Fermi surface in the presence of inversion symmetry [23–25]. Interestingly, the uniform superconducting state is found to support bulk gap nodes on the Fermi surface even

for a constant *s*-wave pairing. From an analogy with the $^3\text{He-A}$ phase, topological superconductivity has been suggested in the former case. We note, however, that the topological superconductivity of WSMs is not a simple generalization of the $^3\text{He-A}$ phase. Indeed, $^3\text{He-A}$ is merely a standard Fermi liquid in the normal state, but WSMs are already topological even in the normal state, supporting Fermi arcs on their boundaries. Furthermore, as inversion-symmetric WSMs require broken time reversal, an electron in the Fermi arcs does not have a Kramers partner, which is necessary to form its BCS Cooper pair. Thus, any uniform pairing state cannot open a gap in the Fermi arcs, keeping them as additional surface gapless modes in the superconducting state. Such additional gapless states do not exist in the $^3\text{He-A}$ phase.

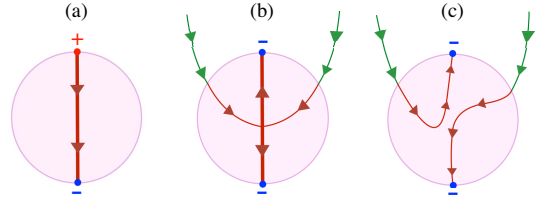


FIG. 1. (color online). Schematic illustration of SABSs in surface momentum space. (a) Surface flat band in $^3\text{He-A}$ phase. Dots indicate the projection of point nodes on the surface BZ. The surface flat bands start smoothly from a projected node with positive monopole charge and end at a projected antinode with negative monopole charge. (b) Crossed surface flat bands in doped superconducting WSMs. The point nodes on the Fermi surface have the same negative monopole charge, so the flat band enters both ends. To preserve the topological flow, the Fermi arcs enter the projected Fermi surface and cross the vertical flat band. (c) Reconnection of flat bands at crossing point. If the system is invariant under magnetic reflection, such reconnection is forbidden.

Actually, we find that the crossed surface flat bands arise from a unique topology of superconducting WSMs. Like Weyl points, nodes in superconducting states generally carry nonzero monopole charges in momentum space. For instance, the $^3\text{He-A}$ phase supports a node–antinode pair with opposite monopole charge in the Fermi surface. Thus, from the surface–bulk correspondence, a surface

flat band starts at the projection of a node on the surface BZ and then ends at that of an antinode.

On the other hand, in the nodal superconducting state in WSMs, each Fermi surface supports only nodes (or only antinodes). Consequently, there must be a topological twist if there is a surface flat band connecting a pair of nodes (or antinodes) with the same monopole charge. Figure 1 illustrates how such a topological twist occurs. A key ingredient is the remaining surface Fermi arcs mentioned above. In the Nambu representation, we have a surface Fermi arc of holes as well as a surface Fermi arc of electrons. Near the Fermi surface, they can merge into the surface flat band, as illustrated in Fig. 1. Consequently, the flat band can be terminated at the projection of a node (or antinode) that has a topological charge identical to that of a node (or antinode) at the starting point. The crossed structure is protected by symmetry of the system. Note that a similar merging of surface states has been reported for superconducting topological insulators [27–29], although the relevant topological number and obtained spectrum are completely different.

In the following, using a concrete model of WSMs, we demonstrate crossed surface flat bands in an s -wave superconducting state. Then, we identify the topological number responsible for the exotic band structure and embody the topological arguments given above.

Model.—As a model of WSMs with an s -wave pairing, we use the two-band Hamiltonian [23, 30],

$$H = \frac{1}{2} \sum_{\mathbf{k}} c_{\mathbf{k}}^{\dagger} \mathcal{H}_{\mathbf{k}} c_{\mathbf{k}}, \quad (1)$$

where the spinor $\hat{c}_{\mathbf{k}}$ is given by $(c_{k_{\uparrow}}, c_{k_{\downarrow}}, c_{-k_{\uparrow}}^{\dagger}, c_{-k_{\downarrow}}^{\dagger})^T$. Further,

$$\begin{aligned} \mathcal{H}_{\mathbf{k}} = & t \sin k_x \sigma_y \tau_z - t \sin k_y \sigma_x \tau_0 + (t_z \cos k_z - M) \sigma_z \tau_z \\ & + m(2 - \cos k_x - \cos k_y) \sigma_z \tau_z - \mu \sigma_0 \tau_z - \Delta \sigma_y \tau_y, \end{aligned} \quad (2)$$

where σ_i (τ_i) is the Pauli matrix in spin (Nambu) space, and t (t_z) is the hopping in the k_x - k_y plane (along the k_z axis). M ($\equiv t_z \cos Q$) denotes a magnetic order or a Zeeman field that breaks the time-reversal symmetry, μ is the chemical potential, and Δ is a conventional s -wave pair potential. We also introduce a parameter m to control the position of the Weyl points. When $m = 0$, the normal state ($\Delta = 0$) possesses four pairs of bands touching Weyl points at $(0, 0, \pm Q)$, $(\pi, 0, \pm Q)$, $(0, \pi, \pm Q)$, and $(\pi, \pi, \pm Q)$, respectively. Hence, upon slight doping with small μ , we have eight disconnected Fermi surfaces, each of which surrounds a Weyl point. When m is turned on, however, the latter three pairs of Weyl points located on the boundary of the BZ move; for large m , they pair-annihilate. Correspondingly, only two disconnected Fermi surfaces surrounding Weyl points at $(0, 0, \pm Q)$ survive.

Each Fermi surface of the doped WSM, in contrast to those of ordinary metals, does not have spin degeneracy

because of the time-reversal breaking and strong spin-orbit interaction. The spin and momentum are locked on the Fermi surface, so a spinless system is realized effectively. In this situation, even an s -wave pairing may host topological superconductivity [31–35]. In the present case, the simplest choice of the pair potential generates point nodes of the superconducting gap at the north and south poles of the Fermi surfaces [23].

Surface Andreev bound states.—Surface Andreev bound states (SABSs) [36–39] are a powerful probe of topological superconductivity because they directly reflect bulk topological structures [40–42]. To identify the nodal topological superconductivity in doped WSMs, we now examine the SABSs. Using an efficient way to calculate the lattice Green's function [43], we can obtain the SABSs from the poles of the Green's function. We choose the surface perpendicular to the x direction.

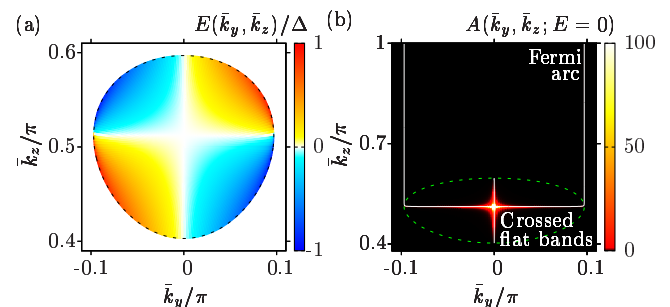


FIG. 2. (color online). SABS in the projected Fermi surface near $(0, 0, Q)$. (a) Energy dispersion $E(\bar{k}_y, \bar{k}_z)$ of SABS. (b) Flat bands of SABS [inside the outline of the projected Fermi surface (green dashed line)] and the Fermi arcs (outside) obtained as poles of spectral function $A(\bar{k}_y, \bar{k}_z; E = 0)$. In both (a) and (b), we choose $t = t_z = 1$, $Q = \pi/2$, $\mu = 0.3$, $\Delta = 0.001$, and $m = 0.8$.

Figure 2(a) shows the obtained SABSs. The model parameters are chosen so that the WSM has only two disconnected Fermi surfaces in the normal state. We show only the SABS in the upper half-plane ($\bar{k}_z > 0$) of the surface BZ, but a similar SABS exists in the lower half-plane ($\bar{k}_z < 0$). Clearly, Fig. 2(a) indicates that the SABS hosts two crossed flat bands extended in the vertical and horizontal directions, respectively.

As in the $^3\text{He-A}$ phase, the vertical flat band is terminated at the projection of gap nodes on the surface BZ. The spectrum in the horizontal direction, however, is very different: For a fixed \bar{k}_z , the SABS appears as a chiral edge mode with a linear dispersion, $E = v(\bar{k}_z)\bar{k}_y$, for small \bar{k}_y . In the $^3\text{He-A}$ phase, the chiral edge mode retains the same sign as its group velocity, but in the present case, the group velocity $v(\bar{k}_z)$ becomes zero at the position of the horizontal flat band, and the sign of $v(\bar{k}_z)$ is reversed when the chiral mode crosses the horizontal flat band. We also find that the horizontal flat band eventually becomes Fermi arcs, as illustrated in Fig. 2(b).

The crossed flat band structure can also be confirmed by quasiclassical analysis. Consider a semi-infinite superconducting WSM placed on the right ($x > 0$) with a semi-infinite insulator on the left ($x < 0$). This can be done by replacing the parameters Δ and M in Eq. (2) with $\Delta\Theta(x)$ and $t_z \cos Q + M_0\Theta(-x)$, respectively. A large M_0 is chosen so that the left side does not have Weyl cones and thus become insulating. For weak pairing $0 < \Delta \ll \mu$, we can use the quasiclassical BdG Hamiltonian,

$$\mathcal{H} = it_z \sin Q \partial_z \sigma_z \tau_z - it(\partial_x \sigma_y \tau_z - \partial_y \sigma_x \tau_0) - \mu \sigma_0 \tau_z - \Delta \Theta(x) \sigma_y \tau_y - M_0 \Theta(-x) \sigma_z \tau_z, \quad (3)$$

near the Weyl point at $(0, 0, Q)$. The solution of the BdG equation $\mathcal{H}\Psi(r) = E\Psi(r)$ is given by $\Psi(r) = e^{i\bar{k}_y y + i(\bar{k}_z - Q)z} [\Psi_I(x)\Theta(-x) + \Psi_S(x)\Theta(x)]$ with

$$\begin{aligned} \Psi_I(x) &= [s_e \Psi_{e1} + s_h \Psi_{h1}] e^{\kappa x}, \\ \Psi_S(x) &= t_e \Psi_{et} e^{ik_x x} + t_h \Psi_{ht} e^{-ik_x x}. \end{aligned} \quad (4)$$

Here $k_x^{e(h)} = \sqrt{q_1^2 - \bar{k}_y^2 - (q_1/q_2)^2 (\bar{k}_z - Q)^2} \pm i\zeta$ and $\kappa t = \sqrt{[(t_z \sin Q)(\bar{k}_z - Q) + M_0]^2 + t^2 \bar{k}_y^2 - \mu^2}$, with $q_1 = \mu/t$, $q_2 = \mu/(t_z \sin Q)$ and $\zeta = \frac{\sqrt{\Delta^2 \sin^2 \beta - E^2}}{t \sin \beta \cos \phi}$. With the parametrization of $\bar{k}_y = q_1 \sin \beta \sin \phi$ and $\bar{k}_z = q_2 \cos \beta + Q$, the four component amplitudes are given by $\Psi_{e1} = [t(\kappa + \bar{k}_y), -\eta, 0, 0]^T$, $\Psi_{h1} = [0, 0, t(-\kappa + \bar{k}_y), \eta]^T$, $\Psi_{et} = [\gamma \tan(\beta/2), i\gamma e^{i\phi}, -ie^{i\phi} \tan(\beta/2), 1]^T$, and $\Psi_{ht} = [\tan(\beta/2), -ie^{-i\phi}, i\gamma e^{-i\phi} \tan(\beta/2), \gamma]^T$, where $\eta = M_0 + \mu + (t_z \sin Q)(\bar{k}_z - Q)$, and $\gamma = \frac{\sqrt{E + \sqrt{E^2 - \Delta^2 \sin^2 \beta}}}{\sqrt{E - \sqrt{E^2 - \Delta^2 \sin^2 \beta}}}$. The coefficients $s_{e(h)}$ and $t_{e(h)}$ and the energy E are determined so as to satisfy the boundary condition $\Psi_I(0) = \Psi_S(0)$. Then, we obtain the energy dispersion as

$$E = \Delta \bar{k}_y (\bar{k}_z - Q) / (q_2 \sqrt{q_1^2 - \bar{k}_y^2}), \quad (5)$$

which clearly shows two flat bands along $\bar{k}_y = 0$ and $\bar{k}_z = Q$, respectively. We also find that the group velocity $v(\bar{k}_z) = \partial E / \partial \bar{k}_z$ reverses its sign at $\bar{k}_z = Q$, as expected.

Topological Analysis.— Now we would like to identify the bulk topology relevant to the crossed surface flat bands, which reveals that the unusual band structure is rather general for nodal superconducting states of WSMs. For simplicity, we consider the simplest case with two disconnected Fermi surfaces separated in the k_z direction, but more complicated cases can be discussed similarly.

As mentioned above, point nodes in superconducting WSMs behave like monopoles in momentum space. Each point node is a source or sink of the flux of the U(1) gauge field, $\mathcal{A}(\mathbf{k}) = i \sum_{E_n < 0} \langle u_n(\mathbf{k}) | \nabla_{\mathbf{k}} | u_n(\mathbf{k}) \rangle$, where $|u_n(\mathbf{k})\rangle$ is a bulk occupied state of the BdG Hamiltonian, and the summation is taken for all occupied states. To capture the topological structure, consider a plane S that is normal to the k_z axis in the BZ.

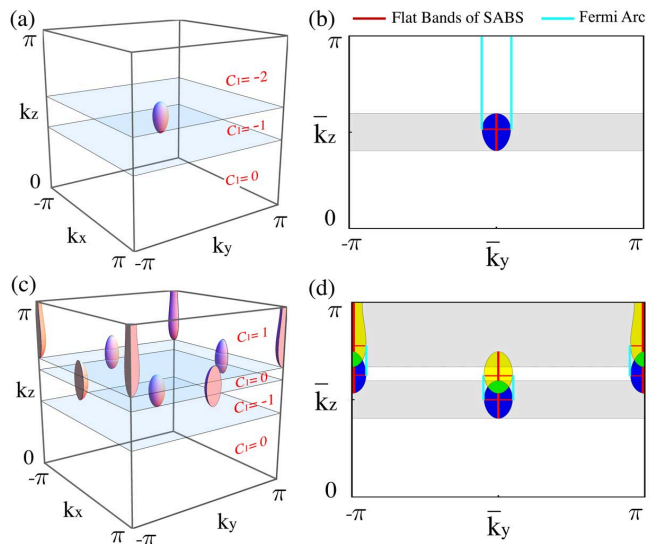


FIG. 3. (color online). Bulk topology and surface states in our model. (a) Fermi surfaces and Chern number at a given k_z in the upper half-BZ for $m = 0.8$. The Chern number $C_1(k_z)$ abruptly changes when k_z crosses a plane including a point node. The amount of change is given by the monopole charge of the point node. (b) Surface states for $m = 0.8$. Solid lines indicate flat bands of SABS and Fermi arcs. Dark shaded region represents the projected Fermi surface. (c) (d) The same plots for $m = 0.2$.

If S does not contain any point nodes, the total flux (over 2π) penetrating S defines the first Chern number, $C_1(k_z) = \frac{1}{2\pi} \int_S d^2k [\nabla_{\mathbf{k}} \times \mathcal{A}(\mathbf{k})]_z$, where k_z is the position of S . The Chern number is a topological invariant that remains the same unless S touches a gap-closing point. When S crosses a point node, however, the Chern number changes. The change is equal to the total flux leaving the point node; thus, it provides its monopole charge.

When S is not close to the Fermi surface, the Chern number can be evaluated rather easily. In this case, we can turn off Δ without gap closing. Therefore, the Chern number is essentially the same as that in the normal state, though we have to take into account the contribution from holes as well as electrons. For inversion-symmetric WSMs, the hole and electron contributions are found to be the same, so the Chern number is doubled. For instance, if the Chern number of electrons is 1 (0) when the projection of S on the surface BZ crosses (does not cross) a Fermi arc, in the superconducting state it becomes 2 (remains 0) if S does not overlap the Fermi surface.

This simple calculation gives an alternative explanation of why the Fermi arcs remain in the superconducting state. From the surface-boundary correspondence, a nonzero bulk Chern number in WSMs ensures the existence of a Fermi arc; thus, if the Chern number is dou-

bled, the number of Fermi arcs is also doubled by adding those of holes. The resulting Fermi arcs remain gapless even in the superconducting state.

Interestingly, the same calculation also explains why point nodes arise in the superconducting state. Because each Fermi surface surrounds a Weyl point, at least two Fermi arcs (i.e., those of holes and electrons) enter the projection of the Fermi surface on the surface BZ. From the above calculation, the Chern number corresponding to the remaining Fermi arcs should be even and nonzero, so a net flux of the U(1) gauge field $\mathcal{A}(\mathbf{k})$ also enters the Fermi surface. Therefore, flux conservation implies that there must be a source or sink of flux near the Fermi surface. In the normal state, the Weyl point is exactly the required source or sink, but in the superconducting state, it cannot be because it is below (or above) the Fermi level, so the Weyl point can no longer provide a monopole charge. Alternatively, we must have an even number of superconducting gap nodes on the Fermi surface, which supply a nonzero total monopole charge.

The above arguments clarify the difference between point nodes in superconducting WSMs and those in $^3\text{He-A}$ phase. For superconducting WSMs, a nontrivial topology in the normal state is essential for the existence of point nodes. Thus, even a topologically trivial s -wave pairing state may support point nodes. In contrast, in the $^3\text{He-A}$ phase, a topologically nontrivial gap function is necessary for the existence of point nodes. Furthermore, the total monopole charge of nodes in the Fermi surface must be nonzero for superconducting WSMs, whereas it is zero for the latter case. Figure 3 shows the Chern numbers and corresponding SABs in our model; the expected topological structures are indeed realized.

Note that the crossed surface flat bands are protected by symmetry of the system. Although time-reversal symmetry is broken in WSMs, a combination of time-reversal and mirror reflection can be preserved, in a manner similar to that in the present model. Actually, we find that WSMs in pyrochlore iridates, HgCr_2Se_4 , and a topological insulator multilayer retain such magnetic mirror reflection symmetry. If the surface of a WSM retains magnetic mirror reflection symmetry, the surface flat bands should be symmetric under the reflection. As illustrated in Fig. 1(c), this symmetry requirement forbids reconnection of flat bands that resolves the crossing point [44].

Experimental Signatures.— To explore the experimental signatures of the newly discovered SABs, we consider a normal metal/superconductor (NS) junction in a doped WSM and calculate the normalized tunneling conductance $\sigma_n(eV) = \sigma_S(eV)/\sigma_N(eV)$ using the tight binding model in Eq. (1) with an appropriate boundary condition [45, 46]. Here $\sigma_S(eV)$ is the conductance of the NS junction, and $\sigma_N(eV)$ is that in the normal state. We denote the transmissivity at the interface by χ , where $\chi = 0$ ($\chi = 1$) corresponds to the low transparent limit (full transmissivity)[46].

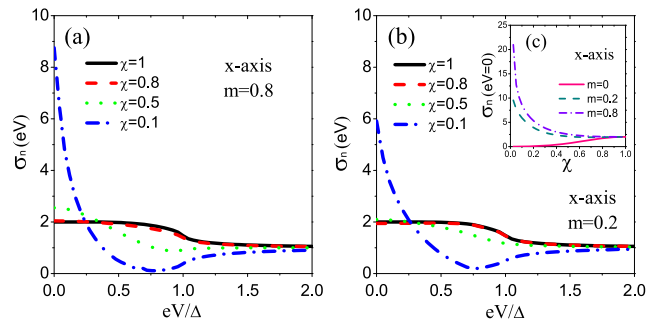


FIG. 4. (color online). Normalized tunneling conductance as a function of bias voltage (eV/Δ) for m equal to (a) 0.8 and (b) 0.2. (c) Relation between height of normalized ZBCP and χ . Other parameters are as the same as in Fig. 2.

Figures 4(a) and (b) show the tunneling conductance σ_n in the x direction. The obtained σ_n shows zero-bias conductance peaks (ZBCPs), where the peak height is inversely proportional to χ , as shown in Fig. 4(c). Such features are rather similar to those of high- T_C cuprates, which support line nodes [39, 47, 48], but not those of Sr_2RuO_4 , which is a superconducting analog of the $^3\text{He-A}$ phase [49] or a ferromagnet/superconductor junction on the surface of a topological insulator [50]. Although the chiral p -wave state supports a vertical flat band, such a huge σ_n at $eV = 0$ cannot be obtained. In contrast, the crossing point of the flat bands in the superconducting WSMs forms a saddle point in the energy dispersion, producing a Van Hove singularity in the surface density of states. As a result, the ZBCP is very prominent.

Summary and Discussions.— In this letter, we reported that WSMs with surface Fermi arcs may support even more exotic crossed surface flat bands in the superconducting state. We found that the nontrivial topology of their normal state results in bulk point nodes in the s -wave pairing state, which enables us to design such nontrivial structure in condensed matter physics.

In closing, we remark on the possible generalization of this work. Our topological arguments require three conditions. The first is a uniform pairing state. A nonuniform pairing state such as the Fulde-Ferrell-Larkin-Ovchinnikov state mixes the Chern numbers with different momenta, so it may destroy the topology of WSMs relevant to the crossed flat bands. The second is broken time-reversal symmetry in WSMs. For time-reversal-symmetric WSMs, the Chern numbers of electrons and of holes are canceled, so superconducting states cannot dominate the nontrivial topology of WSMs. The final condition is magnetic mirror reflection symmetry, which stabilizes the crossed flat bands. Once these three conditions are met, we may have crossed surface flat bands for any pairing state. Although an unconventional Cooper pair may create additional nodes on the Fermi surface, the total number of monopole charges should be nonzero,

which allows the hosting of such complicated flat bands.

We thank A. Yamakage for useful discussion. This work was supported in part by Grants-in-Aid for Scientific Research from the Ministry of Education, Culture, Sports, Science and Technology of Japan (“Topological Quantum Phenomena” No. 22103005 and No. 25287085) and by the EU-Japan program “IRON SEA.”

-
- [1] S. Murakami, *New J. Phys.* **9**, 356 (2007).
 [2] X. Wan, A. M. Turner, A. Vishwanath, and S. Y. Savrasov, *Phys. Rev. B* **83**, 205101 (2011).
 [3] G. Xu, H. Weng, Z. Wang, X. Dai, and Z. Fang, *Phys. Rev. Lett.* **107**, 186806 (2011).
 [4] A. A. Burkov and L. Balents, *Phys. Rev. Lett.* **107**, 127205 (2011).
 [5] W. Witczak-Krempa and Y. B. Kim, *Phys. Rev. B* **85**, 045124 (2012).
 [6] G. Chen and M. Hermele, *Phys. Rev. B* **86**, 235129 (2012).
 [7] H.-J. Kim, K.-S. Kim, J.-F. Wang, V. A. Kulbachinskii, K. Ogawa, M. Sasaki, A. Ohnishi, M. Kitaura, Y.-Y. Wu, L. Li, I. Yamamoto, J. Azuma, M. Kamada, and V. Dobrosavljević, *Phys. Rev. Lett.* **110**, 136601 (2013).
 [8] P. Hosur and X. Qi, *Comptes Rendus Physique* **14**, 857 (2013).
 [9] T. Morimoto and A. Furusaki, preprint, arxiv: 1403.7962 (2014).
 [10] S. L. Adler, *Phys. Rev.* **177**, 2426 (1969).
 [11] J. Bell and R. Jackiw, *Nuovo Cimento A* **60**, 47 (1969).
 [12] H. Nielsen and M. Ninomiya, *Physics Letters B* **130**, 389 (1983).
 [13] A. A. Zyuzin and A. A. Burkov, *Phys. Rev. B* **86**, 115133 (2012).
 [14] C.-X. Liu, P. Ye, and X.-L. Qi, *Phys. Rev. B* **87**, 235306 (2013).
 [15] M. N. Chernodub, A. Cortijo, A. G. Grushin, K. Landsteiner, and M. A. H. Vozmediano, *Phys. Rev. B* **89**, 081407 (2014).
 [16] K. Landsteiner, *Phys. Rev. B* **89**, 075124 (2014).
 [17] Z. Wang and S.-C. Zhang, *Phys. Rev. B* **87**, 161107 (2013).
 [18] H. Ooguri and M. Oshikawa, *Phys. Rev. Lett.* **108**, 161803 (2012).
 [19] Y. Chen, S. Wu, and A. A. Burkov, *Phys. Rev. B* **88**, 125105 (2013).
 [20] C. Fang, M. J. Gilbert, X. Dai, and B. A. Bernevig, *Phys. Rev. Lett.* **108**, 266802 (2012).
 [21] D. Kurebayashi and K. Nomura, *J. Phys. Soc. Jpn.* **83**, 063709 (2014).
 [22] A. A. Burkov and L. Balents, *Phys. Rev. B* **84**, 235126 (2011).
 [23] G. Y. Cho, J. H. Bardarson, Y.-M. Lu, and J. E. Moore, *Phys. Rev. B* **86**, 214514 (2012).
 [24] H. Wei, S.-P. Chao, and V. Aji, *Phys. Rev. B* **89**, 014506 (2014).
 [25] H. Wei, S.-P. Chao, and V. Aji, *Phys. Rev. B* **89**, 235109 (2014).
 [26] V. Shivamoggi and M. J. Gilbert, *Phys. Rev. B* **88**, 134504 (2013).
 [27] T. H. Hsieh and L. Fu, *Phys. Rev. Lett.* **108**, 107005 (2012).
 [28] A. Yamakage, K. Yada, M. Sato, and Y. Tanaka, *Phys. Rev. B* **85**, 180509 (2012).
 [29] S. Takami, K. Yada, A. Yamakage, M. Sato, and Y. Tanaka, *J. Phys. Soc. Jpn.* **83**, 064705 (2014).
 [30] K.-Y. Yang, Y.-M. Lu, and Y. Ran, *Phys. Rev. B* **84**, 075129 (2011).
 [31] M. Sato, Y. Takahashi, and S. Fujimoto, *Phys. Rev. Lett.* **103**, 020401 (2009).
 [32] J. Alicea, *Phys. Rev. B* **81**, 125318 (2010).
 [33] J. D. Sau, R. M. Lutchyn, S. Tewari, and S. Das Sarma, *Phys. Rev. Lett.* **104**, 040502 (2010).
 [34] Y. Oreg, G. Refael, and F. von Oppen, *Phys. Rev. Lett.* **105**, 177002 (2010).
 [35] R. M. Lutchyn, J. D. Sau, and S. D. Sarma, *Phys. Rev. Lett.* **105**, 077001 (2010).
 [36] L. J. Buchholtz and G. Zwicknagl, *Phys. Rev. B* **23**, 5788 (1981).
 [37] J. Hara and K. Nagai, *Prog. Theor. Phys.* **76**, 1237 (1986).
 [38] C. R. Hu, *Phys. Rev. Lett.* **72**, 1526 (1994).
 [39] S. Kashiwaya and Y. Tanaka, *Rep. Prog. Phys.* **63**, 1641 (2000).
 [40] A. P. Schnyder, S. Ryu, A. Furusaki, and A. W. W. Ludwig, *Phys. Rev. B* **78**, 195125 (2008).
 [41] M. Sato, Y. Tanaka, K. Yada, and T. Yokoyama, *Phys. Rev. B* **83**, 224511 (2011).
 [42] Y. Tanaka, M. Sato, and N. Nagaosa, *J. Phys. Soc. Jpn.* **81**, 011013 (2012).
 [43] A. Umerski, *Phys. Rev. B* **55**, 5266 (1997).
 [44] For more detailed topological arguments, see the Supplementary Materials.
 [45] Q.-G. Zhu and H. Kroemer, *Phys. Rev. B* **27**, 3519 (1983).
 [46] See the supplementary materials.
 [47] Y. Tanaka and S. Kashiwaya, *Phys. Rev. Lett.* **74**, 3451 (1995).
 [48] T. Löfwander, V. S. Shumeiko, and G. Wendin, *Supercond. Sci. Technol.* **14**, R53 (2001).
 [49] M. Yamashiro, Y. Tanaka, and S. Kashiwaya, *Phys. Rev. B* **56**, 7847 (1997).
 [50] Y. Tanaka, T. Yokoyama, and N. Nagaosa, *Phys. Rev. Lett.* **103**, 107002 (2009).

Supplementary Materials

S1. Magnetic mirror reflection symmetry

Here we discuss magnetic mirror reflection symmetry in WSMs. The magnetic mirror reflection symmetry is a combined symmetry of mirror reflection and time-reversal. As discussed below, many WSMs naturally have mirror reflection symmetry in a certain direction.

First, it should be noted that broken time-reversal is necessary to obtain a nonzero Chern number $C_1(k_z)$ in inversion symmetric WSMs. At the same time, we would like to point out that for the nonzero Chern number $C_1(k_z)$, reflection symmetries in directions normal to the z -axis must be broken. Because the flux $[\nabla_{\mathbf{k}} \times \mathcal{A}(\mathbf{k})]_z$ is odd under time-reversal and the reflection, each of these symmetries forces the integral $C_1(k_z) = \frac{1}{2\pi} \int d^2k [\nabla_{\mathbf{k}} \times \mathcal{A}(\mathbf{k})]_z$ to be zero.

Although each of them must be broken, their combined symmetry is consistent with inversion symmetric WSMs. Actually, we find that WSMs in pyrochlore iridates and HgCr_2Se_4 retain such magnetic mirror reflection symmetry. In both WSMs, the magnetic mirror reflection with respect to the (110) plane is preserved. This fact could be physically understood as a consequence that magnetic orders of these materials, which are necessary for nonzero $C_1(k_z)$, keep symmetry of the original materials as much as possible. We also find that a WSM in a topological insulator multilayer proposed in Ref.[S1] has a similar magnetic mirror reflection symmetry. Therefore, if Cooper pairs do not break the magnetic reflection symmetry, then the corresponding superconducting phase also retains the magnetic reflection symmetry.

Now we argue the magnetic mirror reflection symmetry in our model,

$$\begin{aligned} \mathcal{H}_{\mathbf{k}} = & t \sin k_x \sigma_y \tau_z - t \sin k_y \sigma_x \tau_0 + (t_z \cos k_z - M) \sigma_z \tau_z \\ & + m(2 - \cos k_x - \cos k_y) \sigma_z \tau_z - \mu \sigma_0 \tau_z - \Delta \sigma_y \tau_y. \end{aligned} \quad (\text{S1})$$

The time-reversal operator is given by

$$T = -i \sigma_y \mathcal{K} \tau_0. \quad (\text{S2})$$

with complex conjugation operator \mathcal{K} , and the mirror reflection operator is given by

$$M_{xz} = i \sigma_y \tau_0, \quad (\text{S3})$$

and each of these symmetries is broken in our model,

$$T \mathcal{H}_{(k_x, k_y, k_z)} T^{-1} \neq \mathcal{H}_{(-k_x, -k_y, -k_z)}, \quad M_{xz} \mathcal{H}_{(k_x, -k_y, k_z)} M_{xz}^{-1} \neq \mathcal{H}_{(k_x, k_y, k_z)}. \quad (\text{S4})$$

However, combining these two operators T and M_{xz} , we can define time-reversal like operator $\tilde{T} = M_{xz} T$, which satisfies

$$\tilde{T} \mathcal{H}_{(k_x, k_y, k_z)} \tilde{T}^{-1} = \mathcal{H}_{(-k_x, k_y, -k_z)}. \quad (\text{S5})$$

This is the magnetic mirror reflection symmetry. Combining with the particle-hole symmetry of the BdG Hamiltonian,

$$C \mathcal{H}_{(-k_x, -k_y, -k_z)} C^{-1} = -\mathcal{H}_{(k_x, k_y, k_z)}, \quad (\text{S6})$$

with

$$C = \sigma_0 \mathcal{K} \tau_x, \quad (\text{S7})$$

we also obtain the *mirror chiral symmetry*

$$\Gamma \mathcal{H}_{(k_x, k_y, k_z)} \Gamma^{-1} = -\mathcal{H}_{(k_x, -k_y, k_z)}. \quad (\text{S8})$$

with

$$\Gamma = C \tilde{T} \quad (\text{S9})$$

This symmetry stabilizes the crossed surface flat bands as illustrated in Fig.1(b) in the main text: Equation (S8) implies that the flat bands with zero energy should be symmetric under $k_y \rightarrow -k_y$. Therefore, a problematic

reconnection process in Fig.1(c) in the main text never happens as far as the magnetic mirror reflection symmetry (and the resultant magnetic chiral symmetry) is present.

S2. Winding number

In this section, we show that the vertical flat band in Fig.2 in the main text has a non-trivial topological number defined by mirror chiral symmetry in Eq.(S8). At $k_y = 0, \pi$, the mirror chiral symmetry reduces to

$$\{\Gamma, \mathcal{H}_{(k_x, k_y, k_z)}|_{k_y=0, \pi}\} = 0, \quad (\text{S10})$$

so we can define the following one-dimensional winding number for fixed k_z [S2],

$$W = -\frac{1}{4\pi i} \int_{-\pi}^{\pi} dk_x \text{tr} [\Gamma \mathcal{H}_{\mathbf{k}}^{-1} \partial_{k_x} \mathcal{H}_{\mathbf{k}}]_{k_y=0, \pi} \quad (\text{S11})$$

Following the discussion in Ref.[S3], we can transform $\mathcal{H}_{\mathbf{k}}$ into anti-diagonalized form by unitary matrix U :

$$U \mathcal{H}_{\mathbf{k}} U^\dagger = \begin{pmatrix} 0 & q(\mathbf{k}) \\ q^\dagger(\mathbf{k}) & 0 \end{pmatrix}, \quad (\text{S12})$$

with

$$q(\mathbf{k}) = \begin{pmatrix} -\mu + D(\mathbf{k}) & -\Delta - it \sin k_x \\ \Delta + it \sin k_x & -\mu - D(\mathbf{k}) \end{pmatrix} \quad (\text{S13})$$

and with $D(\mathbf{k}) = t_z \cos k_z - M + m(2 - \cos k_y - \cos k_x)$. Using a parameter $\theta = \arg(\det q(\mathbf{k}))$, the winding number W at $k_y = 0$ or π can be evaluated as defined as [S4]:

$$W = \frac{1}{2\pi} \int_{-\pi}^{\pi} \frac{\partial \theta}{\partial k_x} dk_x. \quad (\text{S14})$$

After a straightforward calculation, we obtain for $\Delta > 0$

$$W_{k_y=0}(k_z) = \frac{1}{2} [\text{sgn}(\omega_1) - \text{sgn}(\omega_2)], \quad (\text{S15})$$

$$W_{k_y=\pi}(k_z) = \frac{1}{2} [\text{sgn}(\omega_2) - \text{sgn}(\omega_3)], \quad (\text{S16})$$

where $\omega_1 = \Delta^2 + \mu^2 - (t_z \cos k_z - M)^2$, $\omega_2 = \Delta^2 + \mu^2 - (t_z \cos k_z - M + 2m)^2$ and $\omega_3 = \Delta^2 + \mu^2 - (t_z \cos k_z - M + 4m)^2$. In Fig.3(b) in the main text, we find that the winding number is nonzero when k_z is on the vertical flat band at $k_y = 0$. The winding number disappears at point nodes and it remains zero outside the Fermi surface. A more complicated case is also illustrated in Fig.3(d) in the main text.

Similar type of flat bands of SABS as Majorana fermions is discussed in non-centrosymmetric superconductors [S5–S9] and spin-orbit coupled systems[S2, S10–S14].

S3. Tunneling conductance

To calculate the tunneling conductance of NS (normal metal / superconductor) junction based on the tight-binding model in Eqs. (1) and (2) in the main text, we express the Hamiltonian H in a lattice space, which is given by

$$\begin{aligned} H = & \sum_{ijn} it(-\bar{c}_{i,j,n}^\dagger \sigma_y \bar{c}_{i+1,j,n} + \bar{c}_{i,j,n}^\dagger \sigma_y \bar{c}_{i-1,j,n} + \bar{c}_{i,j,n}^\dagger \sigma_x \bar{c}_{i,j+1,n} - \bar{c}_{i,j,n}^\dagger \sigma_x \bar{c}_{i,j-1,n})/2 \\ & + t_z(\bar{c}_{i,j,n}^\dagger \sigma_z \bar{c}_{i,j,n+1} + \bar{c}_{i,j,n}^\dagger \sigma_z \bar{c}_{i,j,n-1})/2 + (2m - t_z \cos Q) \bar{c}_{i,j,n}^\dagger \sigma_z \bar{c}_{i,j,n} \\ & - m(\bar{c}_{i,j,n}^\dagger \sigma_z \bar{c}_{i+1,j,n} + \bar{c}_{i,j,n}^\dagger \sigma_z \bar{c}_{i-1,j,n} + \bar{c}_{i,j,n}^\dagger \sigma_z \bar{c}_{i,j+1,n} + \bar{c}_{i,j,n}^\dagger \sigma_z \bar{c}_{i,j-1,n})/2 \\ & - \mu \bar{c}_{i,j,n}^\dagger \bar{c}_{i,j,n} + \Delta c_{i,j,n\uparrow}^\dagger c_{i,j,n\downarrow} + \Delta c_{i,j,n\downarrow} c_{i,j,n\uparrow}, \end{aligned} \quad (\text{S17})$$

with $\bar{c}_{ijn} = (c_{ijn\uparrow}, c_{ijn\downarrow})^T$. Here, i, j , and n denote the site indexes in x, y and z directions, respectively. We assume the spatial dependence of the pair potential as $\Delta = \Delta_0$ (*zero*) with $i \geq 1$ (< 1) for junctions along x -axis and $\Delta = \Delta_0$ (*zero*) with $n \geq 1$ (< 1) for those along z -axis.

By applying the Bogoliubov transformation in the above lattice Hamiltonian

$$c_{ijn\sigma} = \sum_{\nu} u_{ijn\sigma}^{\nu} \hat{\gamma}_{\nu} + v_{ijn\sigma}^{\nu*} \hat{\gamma}_{\nu}^{\dagger}, \quad (\text{S18})$$

we can obtain the lattice version of the BdG equations

$$\left\{ \begin{array}{l} \varepsilon_\nu u_{ijn\uparrow}^\nu = (-tu_{i+1,jn\downarrow}^\nu + tu_{i-1,jn\downarrow}^\nu + itu_{i,j+1,n\downarrow}^\nu - itu_{i,j-1,n\downarrow}^\nu + t_z u_{ij,n+1\uparrow}^\nu + t_z u_{ij,n-1\uparrow}^\nu)/2 + \\ \quad (2m - t_z \cos Q - \mu) u_{ijn\uparrow}^\nu - m(u_{i+1,jn\uparrow}^\nu + u_{i-1,jn\uparrow}^\nu + u_{i,j+1,n\uparrow}^\nu + u_{i,j-1,n\uparrow}^\nu)/2 + \Delta v_{ijn\downarrow}^\nu, \\ \varepsilon_\nu u_{ijn\downarrow}^\nu = (tu_{i+1,jn\uparrow}^\nu - tu_{i-1,jn\uparrow}^\nu + itu_{i,j+1,n\uparrow}^\nu - itu_{i,j-1,n\uparrow}^\nu - t_z u_{ij,n+1\downarrow}^\nu - t_z u_{ij,n-1\downarrow}^\nu)/2 + \\ \quad (-2m + t_z \cos Q - \mu) u_{ijn\downarrow}^\nu + m(u_{i+1,jn\downarrow}^\nu + u_{i-1,jn\downarrow}^\nu + u_{i,j+1,n\downarrow}^\nu + u_{i,j-1,n\downarrow}^\nu)/2 - \Delta v_{ijn\uparrow}^\nu, \\ \varepsilon_\nu v_{ijn\uparrow}^\nu = (tv_{i+1,jn\downarrow}^\nu - tv_{i-1,jn\downarrow}^\nu + itv_{i,j+1,n\downarrow}^\nu - itv_{i,j-1,n\downarrow}^\nu - t_z v_{ij,n+1\uparrow}^\nu - t_z v_{ij,n-1\uparrow}^\nu)/2 + \\ \quad (-2m + t_z \cos Q + \mu) v_{ijn\uparrow}^\nu + m(v_{i+1,jn\uparrow}^\nu + v_{i-1,jn\uparrow}^\nu + v_{i,j+1,n\uparrow}^\nu + v_{i,j-1,n\uparrow}^\nu)/2 - \Delta u_{ijn\downarrow}^\nu, \\ \varepsilon_\nu v_{ijn\downarrow}^\nu = (-tv_{i+1,jn\uparrow}^\nu + tv_{i-1,jn\uparrow}^\nu + itv_{i,j+1,n\uparrow}^\nu - itv_{i,j-1,n\uparrow}^\nu + t_z v_{ij,n+1\downarrow}^\nu + t_z v_{ij,n-1\downarrow}^\nu)/2 + \\ \quad (2m - t_z \cos Q + \mu) v_{ijn\downarrow}^\nu - m(v_{i+1,jn\downarrow}^\nu + v_{i-1,jn\downarrow}^\nu + v_{i,j+1,n\downarrow}^\nu + v_{i,j-1,n\downarrow}^\nu)/2 + \Delta u_{ijn\uparrow}^\nu. \end{array} \right. \quad (\text{S19})$$

Here, wave functions of the NS junction can be written as

$$\Psi_\alpha^N(\mathbf{r}) = \sum_\beta [\xi_\alpha^e(\mathbf{r}) + r_{\alpha\beta}^e \xi_\beta^e(\mathbf{r}) + r_{\alpha\beta}^h \xi_\beta^h(\mathbf{r})], \quad (\text{S20})$$

$$\Psi_\alpha^S(\mathbf{r}) = \sum_\delta [t_{\alpha\delta}^e \eta_\delta^e(\mathbf{r}) + t_{\alpha\delta}^h \eta_\delta^h(\mathbf{r})], \quad (\text{S21})$$

where α , β and δ denote corresponding Weyl cones. The spinors $\xi^{e(h)}(\mathbf{r})$ and $\eta^{e(h)}(\mathbf{r})$ can be solved by Eq.(S19):

$$\xi^e(\mathbf{r}) = \frac{1}{\sqrt{N_e}} \begin{pmatrix} t(i \sin k_x^e + \sin k_y^e) \\ \mathcal{M}(k_x^e, k_y^e, k_z^e) - \mu - E \\ 0 \\ 0 \end{pmatrix} e^{i(k_x^e x + k_y^e y + k_z^e z)}, \quad (\text{S22})$$

$$\xi^h(\mathbf{r}) = \frac{1}{\sqrt{N_h}} \begin{pmatrix} 0 \\ 0 \\ -t(i \sin k_x^h - \sin k_y^h) \\ -\mathcal{M}(k_x^h, k_y^h, k_z^h) + \mu - E \end{pmatrix} e^{i(k_x^h x + k_y^h y + k_z^h z)}, \quad (\text{S23})$$

with

$$\mathcal{M}(k_x, k_y, k_z) = t_z (\cos k_z - \cos Q) + m(2 - \cos k_x - \cos k_y), \quad (\text{S24})$$

and

$$\eta(\mathbf{r}) = \frac{1}{\sqrt{N_S}} \begin{pmatrix} [\mathcal{G}(p_x, p_y, p_z) - (\mu - E)^2 + \Delta_0^2] (t \sin p_x - it \sin p_y) \\ i [\mathcal{G}(p_x, p_y, p_z) - (\mu - E)^2] [\mu + E - \mathcal{M}(p_x, p_y, p_z)] + [-\mu + E + \mathcal{M}(p_x, p_y, p_z)] \Delta_0^2 \\ i \left\{ -\mu^2 + [E - \mathcal{M}(p_x, p_y, p_z)]^2 - t^2 (\sin^2 p_x + \sin^2 p_y) - \Delta_0^2 \right\} \Delta_0 \\ 2(\mu - \mathcal{M}(p_x, p_y, p_z)) (t \sin p_x - it \sin p_y) \Delta_0 \end{pmatrix} e^{i(p_x x + p_y y + p_z z)}, \quad (\text{S25})$$

with

$$\mathcal{G}(p_x, p_y, p_z) = \mathcal{M}^2(p_x, p_y, p_z) + t^2 (\sin^2 p_x + \sin^2 p_y). \quad (\text{S26})$$

Here, N_e , N_h , and N_S are normalization constants. $k_x^{e(h)}$, $k_y^{e(h)}$ and $k_z^{e(h)}$ satisfy the dispersion relation

$$E^e = \sqrt{\mathcal{G}(k_x^e, k_y^e, k_z^e)} - \mu, \quad (\text{S27})$$

$$E^h = -\sqrt{\mathcal{G}(k_x^h, k_y^h, k_z^h)} + \mu, \quad (\text{S28})$$

and p_x , p_y and p_z satisfy

$$E^S = \sqrt{\left(\mu - \sqrt{\mathcal{G}(p_x, p_y, p_z)} + (\mathcal{M}(p_x, p_y, p_z) \Delta_0 / \mu)^2 \right)^2 + \Delta_0^2 (1 - \mathcal{M}^2(p_x, p_y, p_z) / \mu^2)}. \quad (\text{S29})$$

Using the boundary condition[S15]:

$$\hat{t}\Psi_\alpha^N(i=1) = \chi\hat{t}\Psi_\alpha^S(i=1), \quad (\text{S30})$$

$$\chi\hat{t}'\Psi_\alpha^N(i=0) = \hat{t}'\Psi_\alpha^S(i=0), \quad (\text{S31})$$

for the junction along x -axis and

$$\hat{t}_z\Psi_\alpha^N(n=1) = \chi\hat{t}_z\Psi_\alpha^S(n=1), \quad (\text{S32})$$

$$\chi\hat{t}'_z\Psi_\alpha^N(n=0) = \hat{t}'_z\Psi_\alpha^S(n=0), \quad (\text{S33})$$

for the junction along z -axis, one can obtain the coefficients $r_{\alpha\beta}^{e(h)}$ and $t_{\alpha\delta}^{e(h)}$. Here, \hat{t} and \hat{t}_z represent the effective hopping term in BdG equations given by

$$\hat{t} = (-it\sigma_y\tau_z - m\sigma_z\tau_z)/2, \quad (\text{S34})$$

$$\hat{t}' = (it\sigma_y\tau_z - m\sigma_z\tau_z)/2, \quad (\text{S35})$$

$$\hat{t}_z = \hat{t}'_z = t_z\sigma_z\tau_z/2. \quad (\text{S36})$$

We define χ to describe the transmissivity of NS junction. $\chi = 0$ ($\chi = 1$) corresponds to the edge (perfect transmitting junction). Finally, we obtain the charge current:

$$I(V) = \eta_1 \int dE [f(E - eV) - f(E)] \sigma_S(E), \quad (\text{S37})$$

where

$$\sigma_S(E) = \eta_2 \sum_{\alpha, \mathbf{k}_\parallel} \sigma_S^\alpha(E, \mathbf{k}_\parallel), \quad (\text{S38})$$

$$\sigma_S^\alpha(E, \mathbf{k}_\parallel) = \sum_\beta \text{Re} \left[1 - \frac{v_\beta^{(e)}(E)}{v_\alpha^{(e)}(E)} |r_{\alpha\beta}^e|^2 + \frac{v_\beta^{(h)}(E)}{v_\alpha^{(e)}(E)} |r_{\alpha\beta}^h|^2 \right]. \quad (\text{S39})$$

The summation runs over all the indices of Weyl cones α and \mathbf{k}_\parallel . The quantity \mathbf{k}_\parallel denotes (k_x, k_y) and (k_y, k_z) in the junction along x -axis and that along z -axis, respectively.

$v_\beta^{(e)}(E)$ are the group velocities which can be derived from dispersion relation of the bulk energy spectrum $(1/\hbar)\partial E/\partial k_x$. $\eta_{1(2)}$ is the constant determined by the geometry of the microconstruction. We calculate normalized conductance

$$\sigma_n(eV) = \sigma_S(eV)/\sigma_N(eV), \quad (\text{S40})$$

where $\sigma_N(eV)$ is the conductance in the normal state. It is noted that $\eta_{1(2)}$ does not appear in the expression of the normalized conductance $\sigma_n(eV)$.

In the main text, we have shown that the zero biased conductance peak (ZBCP) emerges when the NS junction is along the x -direction. But as shown in Fig.S1 (a), the present ZBCP depends on m and it vanishes for $m = 0$. This is consistent with the discussion based on the winding number in main text since the projected Fermi surfaces are overlapped and resulting surface Andreev bound states are absent for $m = 0$. In the junction along z -axis, the resulting σ_n is insensitive to m . Since there is no surface Andreev bound states along this direction, ZBCP does not appear in the limit of low transmissivity $\chi \rightarrow 0$. The line shapes of σ_n are the essentially the same as those of the bulk density of states as shown in Fig.S1 (b).

[S1] A. A. Burkov and L. Balents, Phys. Rev. Lett. **107**, 127205 (2011).

[S2] M. Sato and S. Fujimoto, Phys. Rev. B **79**, 094504 (2009).

[S3] A. Ii, K. Yada, M. Sato, and Y. Tanaka, Phys. Rev. B **83**, 224524 (2011).

[S4] M. Sato, Y. Tanaka, K. Yada, and T. Yokoyama, Phys. Rev. B **83**, 224511 (2011).

[S5] P. Goswami and S. Tewari, Phys. Rev. B **88**, 245107 (2013).

[S6] J. D. Sau and S. Tewari, Phys. Rev. B **86**, 104509 (2012).

[S7] R. Queiroz and A. P. Schnyder, Phys. Rev. B **89**, 054501 (2014).

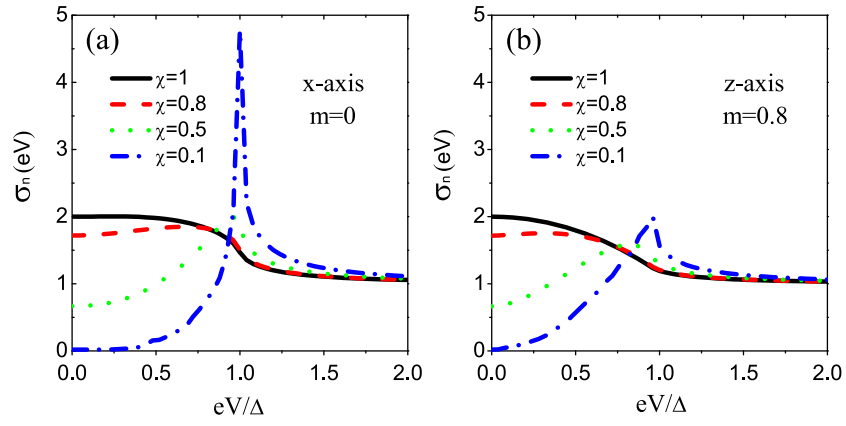


FIG. S1. (Color online) (a) Normalized tunneling conductance as a function of bias voltage (eV/Δ) for junctions along (a) x -axis with $m = 0$ and (b) z -axis with $m = 0.8$. Other parameters are as the same as in Fig.2 in the main text.

- [S8] K. Yada, M. Sato, Y. Tanaka, and T. Yokoyama, Phys. Rev. B. **83**, 064505 (2011).
- [S9] Y. Tanaka, Y. Mizuno, T. Yokoyama, K. Yada, and M. Sato, Phys. Rev. Lett. **105**, 097002 (2010).
- [S10] M. Sato, Y. Takahashi, and S. Fujimoto, Phys. Rev. Lett. **103**, 020401 (2009).
- [S11] J. Alicea, Phys. Rev. B **81**, 125318 (2010).
- [S12] J. D. Sau, R. M. Lutchyn, S. Tewari, and S. Das Sarma, Phys. Rev. Lett. **104**, 040502 (2010).
- [S13] Y. Oreg, G. Refael, and F. von Oppen, Phys. Rev. Lett. **105**, 177002 (2010).
- [S14] R. M. Lutchyn, J. D. Sau, and S. Das Sarma, Phys. Rev. Lett. **105**, 077001 (2010).
- [S15] Q.-G. Zhu and H. Kroemer, Phys. Rev. B **27**, 3519 (1983).